

2007

# Dielectric functions and critical points of PbTiO3, PbZrO3, and PbZr0.57Ti0.43O3 grown on SrTiO3 substrate

T. D. Kang
*Kyunghee University*

Hosun Lee
*Kyunghee University*, hlee@khu.ac.kr

G. Xing
*Virginia Commonwealth University*

***See next page for additional authors***



Kang, T.D., Lee, H., Xing, G., et al. Dielectric functions and critical points of PbTiO3, PbZrO3, and PbZr0.57Ti0.43O3 grown on SrTiO3 substrate. Applied Physics Letters, 91, 022918 (2007). 

# Dielectric functions and critical points of $PbTiO_3$, $PbZrO_3$, and $PbZr_{0.57}Ti_{0.43}O_3$ grown on $SrTiO_3$ substrate

T. D. Kang and Hosun Lee[a)]
*Department of Physics, Kyung Hee University, Yong-In 446-701, Republic of Korea*

G. Xing, N. Izumskaya, V. Avrutin, B. Xiao, and H. Morkoç
*Department of Electrical and Computer Engineering, Virginia Commonwealth University, Richmond, Virginia 23284*

(Received 17 May 2007; accepted 18 June 2007; published online 13 July 2007)

Single crystalline $PbTiO_3$, $PbZrO_3$, and $PbZr_{0.57}Ti_{0.43}O_3$ thin films on $SrTiO_3$ (001) substrates were grown by a combination of molecular beam epitaxy and rf sputtering methods. The authors measured the dielectric functions of the thin films using spectroscopic ellipsometry and determined the interband critical point energies using standard critical point model. They compared the critical point energies to the band structure calculations in the literature. The data suggest that anticrossing behavior occurs between $E_a$ and $E_b$ near Zr=0.17. This phenomenon is attributed to a coupling between $X_{1c}$ and $X_{3c}$ bands caused by intrinsic alloy disorder. © *2007 American Institute of Physics*. [DOI: 10.1063/1.2756168]

Perovskite oxides have very peculiar characteristics of ferroelectricity and piezoelectricity. They can be used in the applications for sensors, nonvolatile random access memories, electro-optic modulators, infrared detectors, and microelectromechanical systems, to cite a few. However, the growth of high quality single crystalline perovskite oxide thin films is very difficult to achieve. Recently, successful growth of $PbTiO_3$,[1] PbZrO3, and $Pb(Zr_xTi_{1-x})O_3$ films[2] on $SrTiO_3$ substrates by using peroxide molecular beam epitaxy (MBE) was reported.

Unlike conventional semiconductors, the dielectric functions and band structures of perovskite oxides have not been studied sufficiently. $PbZr_xTi_{1-x}O_3$ (PZT) is one of the well-known ferroelectric materials and is no exception. The band structure of PZT has been calculated by several groups.[3,4] The dielectric functions and the interband critical points of $PbZr_xTi_{1-x}O_3$ $(0.2 \leqslant x \leqslant 0.8)$ grown on platinized Si substrates by radio frequency sputtering deposition have been reported by Lee *et al.*[4] The interband critical points of PZT $(0 \leqslant x \leqslant 1)$ have been reported by using spectroscopic ellipsometry, reflectivity, and optical transmission by several groups.[4,5] However, definite assignment of the interband critical points has not been carried out yet.

In this work, we measured the dielectric functions of the end-point ternaries $PbTiO_3$ and $PbZrO_3$ and the quaternary $PbZr_{0.57}Ti_{0.43}O_3$ by using spectroscopic ellipsometry. We estimated the interband critical point energies by using standard critical point model,[6] and compared them with the band structure calculations. We assigned the critical point energies in terms of band structure calculations and proposed anticrossing behavior of $E_a$ and $E_b$ critical points near $x=0.17$.

$PbTiO_3$ (PTO) and $PbZrO_3$ (PZO) layers were grown on (001) $SrTiO_3$ (STO) substrates in a Riber 3200 MBE system. A 50% aqueous solution of hydrogen peroxide ($H_2O_2$) was employed as a source of reactive oxygen,[1] and 99.999% pure Pb and 99.995% pure Ti were supplied from double-zone and high-temperature effusion cells, respectively. The layers were grown at an $H_2O_2/H_2O$ pressure of about $5 \times 10^{-5}$ Torr and Pb-to-Ti and Pb-to-Zr flux ratios $\geqslant 1$. Substrate temperatures employed were 600 and 625 °C for PTO and 600 °C for PZO. X-ray diffraction and reflection high energy electron diffraction data indicate that the $PbTiO_3$ and $PbZrO_3$ films are single crystal with the epitaxial relationship of $(001)PbTiO_3$ $(PbZrO_3) \| (001)SrTiO_3$ and $PbTiO_3$ $(PbZrO_3)[100] \| SrTiO_3[100]$. No evidence of *a* domains was found. For more details of the growth of PTO and PZO, we refer to Refs. 1 and 2. We used radio frequency (rf) sputtering to deposit $PbZr_{0.57}Ti_{0.43}O_3$ (PZT57) on STO. The growth temperature was measured to be 750 °C, and rf power was 120 W. The argon and oxygen gas flow rates were 60 and 10 SCCM (SCCM denotes cubic centimeter per minute at STP), respectively.[4,5] The x-ray data showed that the PZT film is single crystal with [001] reflection.[7] The compositions were determined by using energy-dispersive x-ray spectrometry.

We measured the pseudodielectric function of PTO, PZO, and PZT57 grown on $SrTiO_3$ substrate using variable angle spectroscopic ellipsometry at room temperature. We used autoretarder to measure the dielectric function accurately in the transparent region. The angle of incidence was varied as 65°, 70°, and 75°.

Assuming a three phase model of surface roughness, main layer, and STO substrate, we estimated the layer dielectric functions of PTO, PZT57, and PZO using parametric optical constant (POC) model.[8] The POC model provides accurate dielectric function.

Figure 1 depicts the fitted dielectric functions of (a) PTO, (b) PZT57, and (c) PZO layers. The thicknesses of the layers were fitted to be 4.0±0.3 nm for surface roughness layer, and 35.5±0.9 nm for the PTO layer. This is the same for the PZO main layer with 2.1±1.0 nm and 19.8±1.0 nm, respectively, and the same for the PZT57 layer with 2.60±0.05 nm and 587.2±0.5 nm, respectively. The error bar designates 95% reliabilities. Note that the dielectric function is the square of the complex refractive index, that is, $\varepsilon = (n+ik)^2$. The refractive indices are 2.56, 2.55, and 2.40 at 633 nm (1.96 eV) for PTO, PZT57, and PZO, respectively.

a)Author to whom correspondence should be addressed; electronic mail: hlee@khu.ac.kr



 

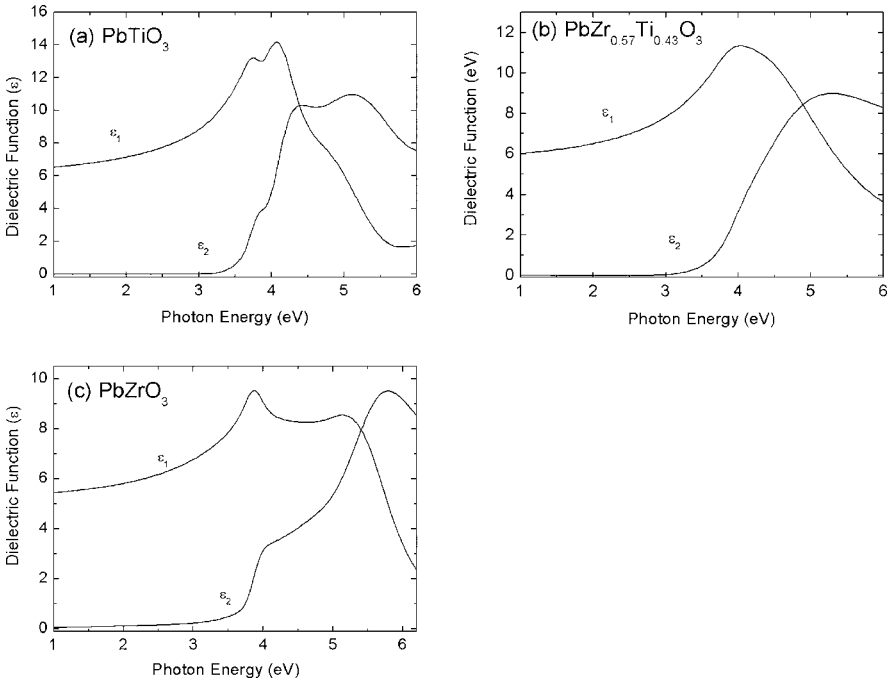


FIG. 1. Fitted dielectric functions ($\varepsilon = \varepsilon_1 + i\varepsilon_2$) of (a) PTO, (b) PZT57, and (c) PZO layer using POC model.

These values are consistent with those reported in the literature.[9] The literature values are between 2.60 and 2.70 for PTO, between 2.44 and 2.54 for PZT50, and between 2.30 and 2.46 for PZO.[9]

Figure 2 exhibits the raw and fitted spectra of the second derivative of the (a) PTO, (b) PZT57, and (c) PZO dielectric functions. We used the standard critical point (SCP) line shape analysis for fitting. The fitted critical point energies are $E_a$=4.11±0.01 eV, $E_b$=3.81±0.01 eV, and $E_c$=5.2±0.1 eV for PTO. The same for PZO are $E_a(E_a)$=3.86±0.01 eV and $E_b$=5.54±0.05 eV.[4,7] In the case of PZT57, $E_a$=3.87 ±0.01 eV and $E_b$=4.42±0.01 eV. The notation of $E_a$, $E_b$, $E_c$ follows Ref. 4. We note that $E_c$ is not observed for PZT except for PTO, and that $E_a$ and $E_c$ may be overlapped for PZO. The increased broadening of the critical point peaks of PZT57 is attributed to alloy disorder.

Our ellipsometric study of PTO, PZT57, and PZO shows the dielectric functions and the electronic band structures of PTO, PZT57, and PZO unambiguously. Several ellipsometric studies of PTO, PZT, and PZO have been reported. Moret *et al.* measured the dielectric functions of PTO, PZT, and PZO grown by metal organic chemical vapor deposition on STO in the spectral range between 1.55 and 3.72 eV by ellipsometry and reflectivity.[9] They estimated the band edge energy as 3.6±0.1 eV for all PZTs, independent of Zr composition, which is near the absorption edge. Therefore, our value $E_b$ =3.81 eV for PTO determined by SCP model is slightly larger than the band edge energy of Moret *et al.* of 3.6 eV. Our value $E_a$=3.86 eV for PZO determined by SCP model is slightly larger than the band edge energy of Moret *et al.* of 3.6 eV.[9] Lee *et al.* calculated the band structures of PTO and PZO, and PZT by using local density approximation

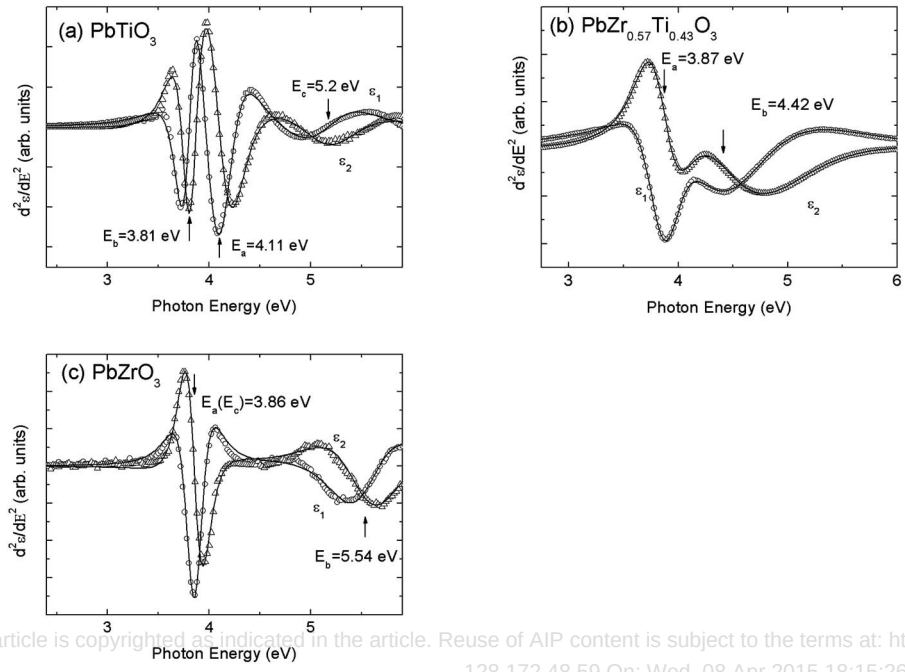


FIG. 2. Raw (discrete symbols) and fitted spectra (sold line) of the second derivatives of the dielectric functions for (a) PTO, (b) PZT57, and (c) PZO using SCP model.

TABLE I. Comparison between the measured and the calculated critical point energies of PZT. Note that the calculated critical point energies of PZT are quoted from Ref. 4.

| Critical point | Interband transitions | Theor. (eV) PTO | Expt. (eV) PTO | Expt. (eV) PZT57 | Expt. (eV) PZO | Theor. (eV) PZO |
|---|---|---|---|---|---|---|
| $E_a$ | $X_{4'v} \rightarrow X_{1c}$ | 4.00 | 4.11(1) | 3.87(1) | 3.86(1) | 3.73 |
| $E_b$ | $X_{5'v} \rightarrow X_{3c}$ | 3.78 | 3.81(1) | 4.42(1) | 5.54(5) | 5.42 |
| $E_c$ | $X_{5'v} \rightarrow X_{1c}$ | 4.93 | 5.2(1) | | 3.86(1) | 4.07 |

method.[4] According to their calculation, there are four interband transitions in the visible-ultraviolet spectral range. They estimated the transition amplitudes and concluded that only three transitions are substantial. As shown in the Table I, the ellipsometrically estimated critical point values agree well with calculated values.

In Fig. 3, we plotted the critical point energies (open symbols) estimated from this work and compared them with the experimental data (closed symbols) and local density approximation (LDA) calculations (dot-dashed lines) of Ref. 3. The experimentally determined critical point peaks are assigned according to the band structure calculations of Lee *et al.*, as shown in Table I.[4] The lowest critical point energy for $PbTiO_3$ ($E_b$=3.78 eV) is attributed to $X_{5'v}-X_{3c}$ transition. The same for $PbZrO_3$ ($E_a$=3.86 eV) is attributed to $X_{4'v}-X_{1c}$ transition. We assigned the critical point peaks of PZT57 at 3.87 and 4.42 eV to $E_a$ and $E_b$, respectively.

Lee *et al.*[4] calculated the band structures of PTO and PZO and estimated the band structure of PZTs by using linear interpolation. Therefore, any possible critical point bowing effect is neglected. The solid lines represent polynomial fitting to the experimental data. The $E_a$ and $E_b$ critical point energies cross near $x$=0.13 according to LDA band structure calculations. However, Fig. 3 suggests that anticrossing is occurring instead of crossing. The anticrossing may be due to the coupling between $X_{1c}$ and $X_{3c}$ bands which may arise from intrinsic alloy disorder. The band energy values for $X_{1c}$ and $X_{3c}$ are 4.10 and 3.84 eV for $PbTrO_3$ and 3.68 and 4.95 eV for $PbZrO_3$, respectively. The potential fluctuation caused by alloy disorder may induce a coupling between the degenerate bands. Although the $X_{1c}$ and $X_{3c}$ conduction band levels cross (i.e., degenerate) near $x$=0.17 in the linear interpolation scheme and even a small perturbation may cause a mixing between the degenerate conduction band states. Similar anticrossing behavior has been reported for semiconductor alloys such as GaInP, GaInNAs, and ZnOSe alloys.[10–12]

In summary, we grew single crystalline $PbTiO_3$, $PbZrO_3$, and $PbZr_{0.57}Ti_{0.43}O_3$ thin films on $SrTiO_3$ (001) substrates by using peroxide molecular beam epitaxy and radio frequency sputtering deposition. We measured the pseudodielectric functions of the thin films using spectroscopic ellipsometry at room temperature and estimated the dielectric functions of

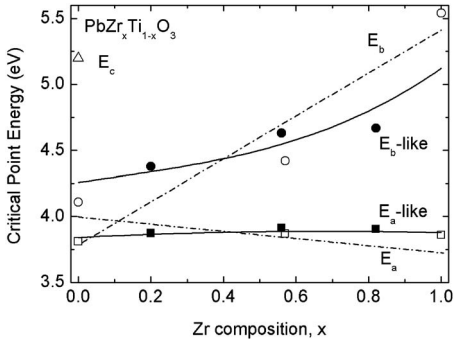


FIG. 3. Critical point energies of PZT as function of Zr composition. The open symbols are our data and the closed symbols are quoted from Ref. 5. The dot-dashed lines are from local density calculations of Ref. 4. The solid lines are from polynomial fitting of experimental data.

the perovskites using parametric semiconductor model. Taking the second order derivative of the fitted dielectric functions, we determined the critical point energies using the standard critical point model. An anticrossing behavior of $E_a$ and $E_b$ critical point energies occurred near Zr=0.17, which may be caused by the coupling between $X_{1c}$ and $X_{3c}$ bands arising from intrinsic alloy disorder.

One of the authors (H.L.) acknowledges the support of Kyung Hee University Research Fund 2007 Grant No. KHU-0764. The work at VCU was funded by a grant from ONR and monitored by C. E. C. Wood.

[1]Xing Gu, N. Izyumskaya, V. Avrutin, H. Morkoç, T. D. Kang, and H. Lee, Appl. Phys. Lett. **89**, 122912 (2006).
[2]N. Izyumskaya, V. Avrutin, Xing Gu, Ü. Özgür, Bo Xiao, Tae Dong Kang, Hosun Lee, and H. Morkoç, in *Ferroelectrics and Multiferroics*, edited by V. Gopalan, J.-P. Maria, M. Fiebig, and C.-W. Nan (MRS, Warrendale, PA, 2007); (Mater. Res. Soc. Symp. Proc. **966E**, paper No. 0966-T11-17.
[3]J. Robertson, W. L. Warren, and B. A. Tuttle, J. Appl. Phys. **77**, 3975 (1995).
[4]Hosun Lee, Youn-Seon Kang, Sang-Jun Cho, Bo Xiao, Hadis Morkoç, Tae Dong Kang, Jingbo Li, Su-Hwai Wei, P. J. Snyder, and J. T. Evans, J. Appl. Phys. **98**, 094108 (2005), and references therein.
[5]Hosun Lee, Youn-Seon Kang, Sang-Jun Cho, Bo Xiao, Hadis, Morkoç, and Tae Dong Kang, Appl. Phys. Lett. **86**, 262902 (2005), and references therein.
[6]P. Lautenschlager, M. Garriga, L. Viña, and M. Cardona, Phys. Rev. B **36**, 4821 (1987), and reference therein.
[7]C. M. Forster, G.-R. Bai, R. Csencsits, J. Vetrone, R. Jammy, L. A. Willis, E. Carr, and J. Amano, J. Appl. Phys. **81**, 2349 (1997).
[8]B. Johs, C. M. Herzinger, J. H. Dinan, A. Cornfeld, and J. D. Benson, Thin Solid Films **313–314**, 137 (1998).
[9]M. P. Moret, M. A. C. Devillers, K. Wörhoff, and P. K. Larsen, J. Appl. Phys. **92**, 468 (2002).
[10]H. Lee, M. V. Klein, L. P. Fu, G. D. Gilliland, H. P. Hjalmarson, D. E. Aspnes, K. C. Hsieh, J. Kim, J. G. Yu, and M. G. Craford, Phys. Rev. B **51**, 4186 (1995).
[11]W. Shan, W. Walukiewicz, J. W. Ager III, E. E. Haller, J. F. Geisz, D. J. Friedman, J. M. Olson, and S. R. Krutz, Phys. Rev. Lett. **82**, 1221 (1999).
[12]W. Shan, W. Walukiewicz, J. W. Ager III, K. M. Yu1, J. Wu, E. E. Haller, and Y. Nabetani, Phys. Status Solidi B **241**, 603 (2004).